Available online at www.sciencedirect.com

ScienceDirect

journal homepage: www.elsevier.com/locate/he

Comparing exergy losses and evaluating the potential of catalyst-filled plate-fin and spiral-wound heat exchangers in a large-scale Claude hydrogen liquefaction process

Geir Skaugen [a], *David Berstad* [a], *Øivind Wilhelmsen* [a,b,*]

[a] *SINTEF Energy Research, Sem Sælands Vei 11, NO-7034, Trondheim, Norway*

[b] *NTNU, Department of Energy and Process Engineering, Kolbjørn Hejes Vei 1B, NO-7491, Trondheim, Norway*

GRAPHICAL ABSTRACT

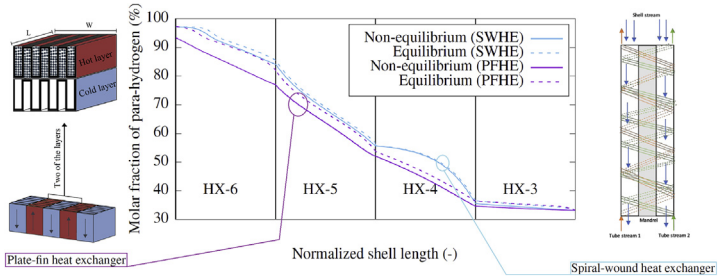

ARTICLE INFO

Article history:
Received 5 November 2019
Received in revised form
7 December 2019
Accepted 11 December 2019
Available online xxx

Keywords:
Hydrogen
Liquefaction
Heat exchanger
Plate-fin
Spiral-wound
Coil-wound

ABSTRACT

Detailed heat exchanger designs are determined by matching intermediate temperatures in a large-scale Claude refrigeration process for liquefaction of hydrogen with a capacity of 125 tons/day. A comparison is made of catalyst filled plate-fin and spiral-wound heat exchangers by use of a flexible and robust modeling framework for multi-stream heat exchangers that incorporates conversion of ortho-to para-hydrogen in the hydrogen feed stream, accurate thermophysical models and a distributed resolution of all streams and wall temperatures. Maps of the local exergy destruction in the heat exchangers are presented, which enable the identification of several avenues to improve their performances.

The heat exchanger duties vary between 1 and 31 MW and their second law energy efficiencies vary between 72.3% and 96.6%. Due to geometrical constraints imposed by the heat exchanger manufacturers, it is necessary to employ between one to four parallel plate-fin heat exchanger modules, while it is possible to use single modules in series for the spiral-wound heat exchangers. Due to the lower surface density and heat transfer coefficients in the spiral-wound heat exchangers, their weights are 2–14 times higher than those of the plate-fin heat exchangers.

* *Corresponding author*. SINTEF Energy Research, Sem Sælands vei 11, NO-7034, Trondheim, Norway.
E-mail address: oivind.wilhelmsen@ntnu.no (Ø. Wilhelmsen).

https://doi.org/10.1016/j.ijhydene.2019.12.076

0360-3199/© 2019 The Authors. Published by Elsevier Ltd on behalf of Hydrogen Energy Publications LLC. This is an open access article under the CC BY license (http://creativecommons.org/licenses/by/4.0/).

Please cite this article as: Skaugen G et al., Comparing exergy losses and evaluating the potential of catalyst-filled plate-fin and spiral-wound heat exchangers in a large-scale Claude hydrogen liquefaction process, International Journal of Hydrogen Energy, https://doi.org/10.1016/j.ijhydene.2019.12.076

In the first heat exchanger, hydrogen feed gas is cooled from ambient temperature to about 120 K by use of a single mixed refrigerant cycle. Here, most of the exergy destruction occurs when the high-pressure mixed refrigerant enters the single-phase regime. A dual mixed refrigerant or a cascade process holds the potential to remove a large part of this exergy destruction and improve the efficiency. In many of the heat exchangers, uneven local exergy destruction reveals a potential for further optimization of geometrical parameters, in combination with process parameters and constraints.

The framework presented makes it possible to compare different sources of exergy destruction on equal terms and enables a qualified specification on the maximum allowed pressure drops in the streams. The mole fraction of para-hydrogen is significantly closer to the equilibrium composition through the entire process for the spiral-wound heat exchangers due to the longer residence time. This reduces the exergy destruction from the conversion of ortho-hydrogen and results in a higher outlet mole fraction of para-hydrogen from the process.

Because of the higher surface densities of the plate-fin heat exchangers, they are the preferred technology for hydrogen liquefaction, unless a higher conversion to heat exchange ratio is desired.

© 2019 The Authors. Published by Elsevier Ltd on behalf of Hydrogen Energy Publications LLC. This is an open access article under the CC BY license (http://creativecommons.org/licenses/by/4.0/).

Introduction

Hydrogen has the potential to become an important, carbon-free energy commodity that can enable low- or zero-emission energy use in several of the world's energy sectors, such as power generation, road and rail transport, sea transport and energy- and emission-intensive industries [1]. Hydrogen can be produced from several energy sources, both renewable and fossil. On the renewable side, water electrolysis using wind and solar energy has a high potential [2]. Fossil energy, primarily natural gas and coal, can be efficiently converted to hydrogen, and the emissions can be reduced to low levels with capture and storage of the CO_2 [2]. A major challenge in a mass roll-out scenario for hydrogen is to achieve energy- and cost-efficient storage, transport and distribution from its origin to end users. Distribution of large quantities across long distances favors dense-phase transport [3]. A promising method for dense-phase transport, both from a cost and energy point-of-view is liquid hydrogen (LH_2) [4,5].

Until now, the market for LH_2 has been small and few resources have been allocated to research and development. Therefore, the hydrogen liquefaction process has a large potential for improvement. A typical capacity of current hydrogen liquefaction plants is 5–30 tons per day (tpd) [4]. In comparison, plants for production of Liquefied natural gas (LNG) have capacities exceeding 10 000 tpd. The industry has recently targeted development of large-scale hydrogen liquefaction plants with capacities exceeding 500 tpd [6].

A key challenge in developing large-scale hydrogen liquefaction plants is to achieve cost and energy-efficient design of the main heat exchangers [7]. The state-of-the-art technology today is plate-fin heat exchangers with catalyst placed in part of the layers to speed up the conversion between ortho- and para-hydrogen [8–10]. In large-scale LNG processes, spiral-wound heat exchangers are a frequently used alternative to plate-fin heat exchangers [11]. In spiral-wound heat exchangers, also referred to as coil-wound heat exchangers, the hot streams flow in pipes wounded around an inner mandrel, and the refrigerant flows counter-currently at the shell side. Spiral-wound heat exchangers are scalable, easy to maintain and have high overall heat transfer coefficients. They are also known to be robust towards thermal expansion, which is crucial as the hydrogen liquefaction process operates down to 20 K. The primary aim of this work is to evaluate the performance and potential of novel catalyst filled spiral-wound heat exchangers in a large-scale hydrogen liquefaction process.

Heat exchangers can be studied with different methods such as experiments [11–14], computational models [15–17] and theory [18,19]. Computational fluid dynamics (CFD) is capable of resolving the flow pattern in the heat exchanger [20–22] and is an excellent tool for obtaining information about local heat transfer and momentum transfer characteristics [22]. At the other side of the spectrum lies the Effectiveness-NTU and LMTD approaches, where effective *UA*-values account for the overall heat transfer characteristics [16,17]. This is the method of choice for demanding process simulations and optimization studies [4,9,23–25]. The best methodology to evaluate the influence of key geometrical parameters on the design of novel multistream heat exchangers lies arguably between CFD and the NTU/LMTD-approaches [26], both with respect to computational complexity and resolution.

In this work, we combine process simulations with the flexible and robust heat exchanger modeling framework presented in Refs. [15,27]. One-dimensional balance equations for mass, energy and momentum are solved for all relevant streams. The streams interact via surface nodes equipped with wall temperatures that build the geometry of the heat exchanger and ensure that no unphysical temperature-

Please cite this article as: Skaugen G et al., Comparing exergy losses and evaluating the potential of catalyst-filled plate-fin and spiral-wound heat exchangers in a large-scale Claude hydrogen liquefaction process, International Journal of Hydrogen Energy, https://doi.org/10.1016/j.ijhydene.2019.12.076

crossing between any streams can occur. State-of-the-art thermo-physical models and correlations are used to account for local heat and momentum transfer. The complete model constitutes a large-set of differential and algebraic equations that must be solved numerically.

We will compare catalyst filled plate-fin heat exchangers and spiral-wound heat exchangers; their size, weight and efficiency. Maps of the local exergy destruction in the heat exchangers will be presented. They reveal several avenues to further improve the process.

The process design and the five main heat exchangers

The hydrogen liquefier considered in this work is a Claude-type liquefaction cycle with a hydrocarbon-based single mixed-refrigerant (MR) pre-cooling cycle. The liquefier has a net capacity of 125 tpd. The overall process flow diagram is shown in Fig. 1. Aspen HYSYS was used to build the simulation model, assuming steady-state operation.

The hydrogen (H_2) feed stream has a pressure of 20 bar and is fed to heat exchanger 1 (HX-1), where it is precooled to approximately 114 K by the single MR cycle. Single MR refrigeration is a mature technology for LNG applications, but has not yet been realized commercially for LH_2, where open nitrogen pre-cooling is the standard [4]. The high-pressure level in the MR cycle at the HX-1 inlet is 35 bar and the required mass flow rate of the refrigerant is about 1600 tpd. After internal cooling to about 114 K, the sub-cooled high-pressure stream is throttled to 4.25 bar, which gives a temperature of 112 K and a vapor fraction of 6% on a molar basis. The low-pressure MR stream has sufficient refrigeration capacity for pre-cooling the high-pressure MR as well as the H_2 feed stream.

One of the main advantages of using MR is the gliding temperature profiles occurring during condensation at high pressure and boiling at low pressure. The single MR composition used in the liquefaction process is given in Table 1. The operating temperature range for the precooling cycle is downwards constrained by the freezing point of the heavier components in the refrigerant mixture. In the present case, the component with the highest freezing point is n-butane, and a certain safety margin between operating temperatures and freeze-out temperature must be maintained. Using the freezing point evaluation tool embedded in Aspen HYSYS, the margin between the actual stream temperature and the estimated n-butane freeze-out temperature is found to be 8.9 K on the high-pressure side, and correspondingly 7.6 K on the low-pressure side in the cold end of HX-1.

Upon evaporation, superheating and returning to the hot end of HX-1, the MR return stream is compressed to 11 bar in the first compression stage. The volume flow at the compressor inlet is about 11 000 m^3/h and the compressor isentropic efficiency is assumed to be 85%. Intercooling between the compression stages causes condensation of a fraction of the refrigerant mixture, predominantly the heaviest component n-butane. A receiver located downstream of the intercooler separates the phases so that they are further compressed to the high-pressure level (35.2 bar) by vapor compression and liquid pumping, before the phases are fed to the HX-1 inlet. The isentropic efficiency for the second compressor stage and pump is assumed to be 85% and 75%, respectively.

HX-2 is the second heat exchanger in the liquefier, operating between ambient temperature and pre-cooling temperature levels. HX-2 pre-cools the high-pressure H_2 stream of the Claude cycle against heating of returning low- and intermediate-pressure cold H_2 streams from the same Claude cycle. The high-pressure stream has a feed temperature and pressure of 288 K and 29.8 bar, respectively. The mass flowrate is 1173 tpd, that is, 9.4 times that of the H_2 feed stream. This mass flowrate balances against those of the returning low- and intermediate-pressure cold H_2 streams in the closed-loop Claude cycle, with flowrates of 51.5 tpd and 1121.5 tpd, respectively. The high-pressure stream is cooled to about 119.5 K, while the cold-stream temperatures approach that of the high-pressure inlet temperature before returning to the H_2 compressors.

After precooling in HX-1, the H_2 feed stream passes through a regenerative fixed-bed catalyst-filled reactor in which a certain fraction of ortho-hydrogen is converted to para-hydrogen. The conversion is assumed to be adiabatic and at the point of equilibrium at the reactor outlet. For an inlet temperature of 114 K and a para-hydrogen fraction of 0.25, the corresponding equilibrium outlet temperature is about 118 K, and the para-hydrogen mole fraction is increased from 0.25 to about 0.33.

In HX-3, the H_2 feed as well as the high-pressure Claude cycle stream are further cooled to about 106 K and 113 K against the returning low- and intermediate-pressure H_2 streams in the Claude cycle. Through the rest of the major heat exchangers in the liquefier, from HX-3 through HX-6, the conversion of ortho-hydrogen to para-hydrogen in the H_2 feed stream occurs inside catalyst-filled channels as the feed stream is cooled further. No catalyzed ortho-to-para conversion takes place in the channels of the high-, intermediate- and low-pressure streams.

On the cold side of HX-3, HX-4 and HX-5, a side stream is withdrawn from the high-pressure line. Each side stream is expanded in cryogenic turbines in respective Brayton branches. They bypass the adjacent heat exchanger and are fed to the cold side of it, as shown in the process flow diagram in Fig. 1. The outlet pressure for the three different expander triplet or pairs matches the pressure level of the intermediate-pressure return line, and the enthalpy drop and thus discharge temperature matches reasonably well the cold-side feed temperature level of the adjacent heat exchanger. All cryo-expanders are assumed to have 85% isentropic efficiency, which is a reasonable assumption based on state-of-the-art technology [28]. The shaft power generated in each liquefier block is about 2.8 MW. Given the large capacity of the liquefier, it is assumed that the shaft power is recovered as electric energy on the outside of the cryogenic coldbox with an overall shaft-to-electricity conversion efficiency of 80%.

In addition to the three Brayton branches, which account for more than 95% of the total flow rate of the Claude cycle high-pressure stream, a Joule-Thomson branch is needed to provide refrigeration capacity in the condensing and sub-cooling heat exchanger, HX-6. To reach the required cold-

Please cite this article as: Skaugen G et al., Comparing exergy losses and evaluating the potential of catalyst-filled plate-fin and spiral-wound heat exchangers in a large-scale Claude hydrogen liquefaction process, International Journal of Hydrogen Energy, https://doi.org/10.1016/j.ijhydene.2019.12.076

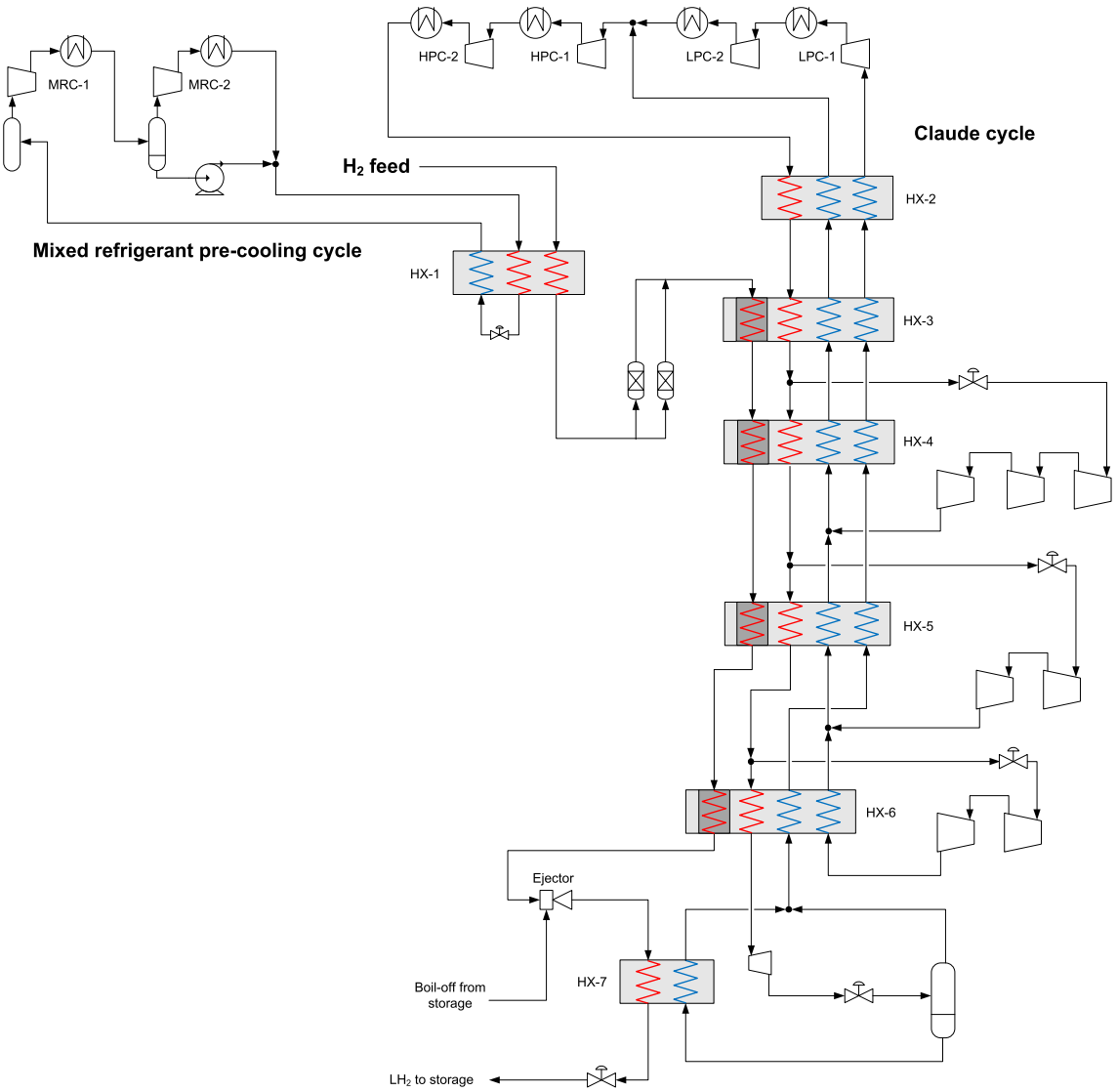

Fig. 1 – Process flow diagram for the 125 tpd hydrogen liquefier.

Table 1 – Mixed refrigerant composition.

Component	Mol. fraction
Nitrogen	0.101
Methane	0.324
Ethane	0.274
Propane	0.031
n-Butane	0.270

side sub cooler temperature, the remaining fraction of the high-pressure H_2 stream is expanded to 1.33 bar in two stages. In the first stage, a liquid expander with 80% isentropic efficiency reduces the pressure to about 7.2 bar in the liquid phase, followed by isenthalpic throttling to 1.33 bar. The sequence of a liquid expander and isenthalpic throttling valve generates considerably less entropy than a single isenthalpic throttling, and therefore a lower vapor fraction. The resulting two-phase H_2 stream enters a receiver serving a flooded evaporator, represented by HX-7, in which a column of LH_2 continuously boils off while it condenses and sub-cools the incoming H_2 feed stream.

The H_2 feed stream is cooled to about 30 K at the outlet of HX-6 before expanded in an ejector, which re-compresses a smaller suction stream of boil-off gas from the LH_2 storage. The ratio between the suction stream and the motive stream, commonly denoted the entrainment ratio of the ejector, is 0.057. The ejector discharge pressure is 1.85 bar, and the resulting vapor fraction of the discharge stream is approximately 0.29. In the flooded evaporator HX-7, the ejector discharge stream is condensed and subcooled by a margin of approximately 1 K before being transferred to the LH_2 storage.

Mathematical models for the heat exchangers

Catalyst must be placed inside the heat exchangers to speed up the kinetics of the following spin-isomer reaction:

$$H_{2,o} \rightleftharpoons H_{2,p}, \quad (1)$$

Please cite this article as: Skaugen G et al., Comparing exergy losses and evaluating the potential of catalyst-filled plate-fin and spiral-wound heat exchangers in a large-scale Claude hydrogen liquefaction process, International Journal of Hydrogen Energy, https://doi.org/10.1016/j.ijhydene.2019.12.076

where subscripts o and p refer to ortho- (where the spin of the protons are the same) and para-hydrogen (where the spins of the protons are opposite). With no catalyst, the heat that is generated when liquefied ortho-hydrogen converts to para-hydrogen in e.g. storage tanks will lead to full evaporation, since the enthalpy difference of ortho-para conversion exceeds the latent heat of evaporation at low temperatures. Therefore it is necessary to convert all the H_2 to para-hydrogen before storage, which will require additional refrigeration capacity and more heat transfer area.

In the following, we will describe the mathematical models used to represent and investigate plate-fin and spiral-wound heat exchangers.

The plate-fin heat exchanger

The plate-fin heat exchanger depicted in Fig. 2 is constructed from layers with fins separated by parting sheets, where cold and hot streams flow counter currently in alternating layers. For layer j of a plate-fin heat exchanger, located between the layers $j-1$ and $j+1$, the steady-state energy balances are:

$$\frac{dh_j}{dz} = \frac{\gamma_j}{2\dot{m}_j}\left(J_{q,j-1,j} + J_{q,j+1,j}\right). \tag{2}$$

Here, h_j denotes the specific enthalpy, $\dot{m}_j$ the mass flow-rate, γ_j the perimeter within layer j and $J_{q,i,j}$ denotes the heat flux from stream i to stream j, where $J_{q,i,j} = -J_{q,j,i}$. The factor $(1/2)$ in Eq. (2) reflects that the perimeter of a layer interacts with two other layers, the layer above and the layer below, where half of the overall perimeter is attributed to each. The momentum balances of all sections can be simplified in terms of differential equations for the pressure

$$\frac{dp_j}{dz} = -f_j \frac{\dot{m}_j^{\,2}}{2A_j^2 \rho_j D_{h,j}}, \tag{3}$$

where p is the pressure, f is the Darcy-Weisbach friction factor, A the cross section area, $D_{h,j}$ is the hydraulic diameter of layer j and ρ the density. Both the heat transfer coefficient and the friction factor depended on whether boiling/condensation occurs, if the fluids are single-phase, and if the fluid was in an open channel, or a channel packed with catalyst pellets. Moreover, the mechanisms for transfer of energy and momentum depended on whether the flow was in the laminar or in the turbulent regimes. To take into account the changing conditions in the heat exchanger, heat transfer coefficients and friction factors based on empirical expressions were used. The heat transfer coefficient for finned geometries is typically represented with a j-factor. For serrated fins, the j-factor and friction factor correlations by Manglik and Bergels [29]. The j-factor is related to the heat transfer coefficient of an open channel through the Stanton and Prandtl numbers [30], where the Nusselt number is linear in the heat transfer coefficient. The heat transfer coefficient for rectangular fins can be obtained by using the correlation by Gnielinski [31], with the friction factor from the correlation by Filonenko [32]. Perforated fins can be treated as plain fins, but with the surface multiplied by a perforation factor of 0.95, meaning that 5% of the area is lost due to perforation, and with the friction factor increased by 20% as recommended by Hesselgreaves [19]. We refer to Ref. [7] for further details.

The sprial-wound heat exchanger

The spiral-wound heat exchanger depicted in Fig. 3 is constructed by tubes wounded around an inner mandrel surrounded by an outer shell. Usually, the hot streams flow inside the wounded pipes and the refrigerant stream flows counter-currently on the shell-side. The helix angle of the various hot

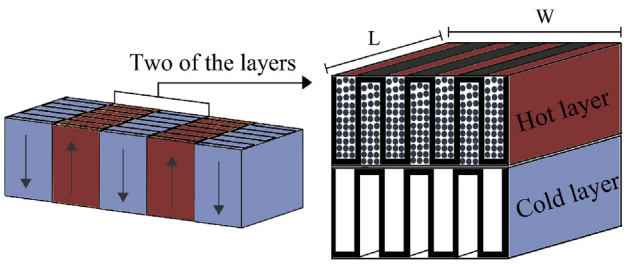

Fig. 2 – An illustration of a plate-fin heat exchanger, where some of the layers are filled with catalyst and hot and cold streams flow in opposite directions. The layers have length, L and width W. For multistream plate-fin heat exchangers, the configuration of hot and cold layers is likely to deviate from the illustration.

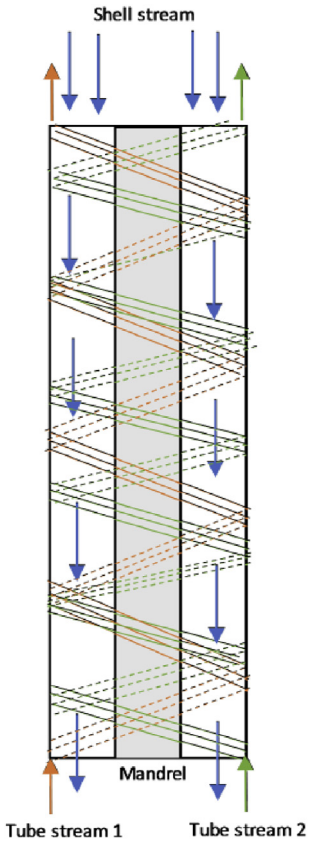

Fig. 3 – An illustration of a spiral-wound heat exchanger, where the pipes are wounded around an inner mandrel. The refrigerant (blue) flows at the shell-side, counter-currently with the streams flowing in the pipes. The helix angle of the pipes of tube stream 1 and tube stream 2 are different to achieve different thermal lengths.

Please cite this article as: Skaugen G et al., Comparing exergy losses and evaluating the potential of catalyst-filled plate-fin and spiral-wound heat exchangers in a large-scale Claude hydrogen liquefaction process, International Journal of Hydrogen Energy, https://doi.org/10.1016/j.ijhydene.2019.12.076

streams can be chosen differently to have different thermal lengths, as illustrated in the figure. The recommendations from Refs. [33,34] have been used as the basis for the modeling. In the model implemented, each stream can be represented by many parallel tubes with the same length, helix angle and other characteristics. The helix angle, β and the longitudinal pitch, P_l are related to the shell and tube lengths and the radial pitch, P_r as

$$\beta_j = \sin^{-1}\left(\frac{L_{shell}}{L_j}\right), \tag{4}$$

$$P_l = 2\pi P_r \cdot \tan(\beta_j), \tag{5}$$

where subscript j refers to tube j and L refers to the total length. The spiral-wound geometry can be characterized by the following parameters: Bundle height, the longitudinal pitch(es), the radial tube pitch, an estimation for the core diameter and an estimation on the number of parallel tubes for each tube stream.

Based on the initial core diameter, an initial number of tubes for the first layer can be calculated. For each additional layer, the layer diameter is computed and an even number of tubes in this layer is calculated and added to the total. The number of layers is increased by one until the total (estimated) number of tubes has been placed.

The total number of layers is found and the outer diameter of the shell can be calculated. The helix angle in each layer will vary slightly around the average helix angle (and longitudinal tube pitch) for the given tube stream, but this is not accounted for in the thermal model that only uses the total heat transfer surface and the average longitudinal tube pitch. The tube increment from one layer to the next will typically be either 0, 1 or 2. When winding up the streams, the layers will alternate between the specified tube streams. The actual radial position of a stream in the bundle is not accounted for in the thermal model, which only uses a one dimensional approach. The differential equations for the spiral-wound heat exchanger are similar to those of the plate-fin heat exchanger, except that all streams (subscript j) heat exchange with the shell-side, and the shell-side heat exchange with all other streams.

Shell side cross flow area

The cross flow area for a helical tube bundle is a mix of in-line and staggered tube arrangements. There are a few methods proposed in the literature that account for this [35]. The method by Gilli [12] is often used to correct the free flow area. The cross flow area is then calculated by using the average diameter between the shell and the core multiplied with the number of layers and the free space distance, S. The cross free-flow area is important, since it is used to calculate the mass flux that will determine the local Re-number used in heat transfer coefficient and friction factor correlations. It is given by:

$$A_{cross} = \pi \cdot \frac{D_{shell} + D_{core}}{2} \cdot N_{layers} \cdot S, \tag{6}$$

where S can become in-line, staggered or calculated from a selected geometry model, i.e. the model by Ref. [12].

$$S_{in-line} = P_r - D_t, \tag{7}$$

$$S_{staggered} = \sqrt{P_r^2 + 0.25P_l^2} - D_t. \tag{8}$$

In the model developed in this work, an alternative method to that presented by Gilli is used, namely the one proposed by Smith [35]. Here, the flow area is calculated directly as the annular area between the core and the shell. The method is shown in Eqs. (9–14) and uses two correction factors. One for the face area, Eq. (11), and one for the helix angle, Eq. (12). It was implemented as described in Ref. [33].

$$A_m = A_a \cdot \frac{A_s}{A_a} \cdot \frac{A_m}{A_s}, \tag{9}$$

$$A_a = \frac{\pi}{4}\left(D_s^2 - D_c^2\right), \tag{10}$$

$$\frac{A_s}{A_a} = 1.0 - D \Big/ P_r, \tag{11}$$

$$\frac{A_m}{A_s} = \frac{\frac{P_r}{2}\sqrt{b} + P_r^2 \ln\left(a + \sqrt{b}\right) \Big/ P_l - D}{P_r - D_t}, \tag{12}$$

$$b = a^2 + 1, \tag{13}$$

$$a = \frac{P_l}{2P_r}. \tag{14}$$

To predict the thermal-hydraulic behavior of the heat exchanger, sub-models for heat transfer coefficients and friction factors are required. For the heat transfer and pressure loss in a spiral-wound heat exchanger, we have implemented the most commonly used models from the literature, typically used in LNG processes [33,34], except when the pipes are filled with catalyst.

Shell side heat transfer

Downward flow has been assumed for the shell side stream. For the MR pre-cooling cycle, the low pressure MR-stream will be on the shell side. For a process where H_2 is used as refrigerant, the medium pressure gas will be the cold fluid flowing at the shell-side. This fluid will be single-phase gas. The single phase heat transfer coefficient has been calculated by using the equation by Gnielinski [33]. The Nusselt number, Nu, was correlated using a laminar and turbulent contribution together with a tube arrangement factor, f_A

$$Nu = \frac{\alpha \cdot X}{\lambda} = f_A \cdot \left(0.3 + \sqrt{Nu_{lam}^2 + Nu_{turb}^2}\right). \tag{15}$$

The characteristic length, X is defined as: $\pi D_t/2$ where D_t is the outside tube diameter. The turbulent and laminar Nu numbers have been calculated from Eqs. (16) and (17) with the Re-number defined from Eq. (18)

$$Nu_{lam} = 0.664 \cdot \sqrt{Re} \cdot Pr^{1/3}, \tag{16}$$

$$Nu_{turb} = \frac{0.037 \cdot Re^{0.8} \cdot Pr}{1 + 2.443 \cdot Re^{-0.1} \cdot \left(Pr^{2/3} - 1\right)}, \tag{17}$$

Please cite this article as: Skaugen G et al., Comparing exergy losses and evaluating the potential of catalyst-filled plate-fin and spiral-wound heat exchangers in a large-scale Claude hydrogen liquefaction process, International Journal of Hydrogen Energy, https://doi.org/10.1016/j.ijhydene.2019.12.076

$$\mathrm{Re} = \frac{u \cdot X \cdot \rho}{\gamma \cdot \mu}, \tag{18}$$

where u is the velocity in the empty cross section, γ is the void fraction used to calculate the average velocity between the tubes and Pr is the Prandtl number. The void fraction, γ and the arrangement factor, f_A have been calculated as for an in-line tube bank from Eqs. (19–24), where P_r and P_l are the radial and longitudinal tube pitches. When the streams have different tube lengths, the helix angle and longitudinal tube pitch will vary. For these circumstances, the bundle average longitudinal pitch is used in Eq. (22)

$$\gamma = 1 - \frac{\pi}{4.0 \cdot a}, \quad b < 1 \tag{19}$$

$$\gamma = 1 - \frac{\pi}{4.0 \cdot ab}, \quad b > 1 \tag{20}$$

$$a = \frac{P_r}{D_t}, \tag{21}$$

$$b = \frac{P_l}{D_t}, \tag{22}$$

$$f_A = 1 + \frac{0.7 \cdot (b/a - 0.3)}{\gamma^{1.5} \cdot (b/a + 0.7)^2}, \quad \text{in-line} \tag{23}$$

$$f_A = 1 + \frac{2}{3b}. \quad \text{staggered} \tag{24}$$

Shell side pressure loss

The shell side pressure loss for single phase gas has been calculated by using the method of Barbe [36]. This is an implicit formulation for the friction factor that combines both in-line and staggered tube arrangement geometries.

$$\left[\frac{dp}{dl}\right]_f = F \cdot \frac{\dot{M}^2}{2 \cdot \rho \cdot P_l}. \tag{25}$$

The mass flux, $\dot{M}$ has been calculated as the mass flow (kg/s) divided by the calculated cross flow area based on in-line, staggered or the method by Gilli, Glaser or Smith. This mass flux is also used in the Re-number in Eq. (29), which differs from the Re-number used in the heat transfer calculations. The friction factor, F, is:

$$F = \frac{2}{\frac{1}{\sqrt{F_{in}}} + \frac{1}{\sqrt{F_{st}}}}. \tag{26}$$

The in-line and staggered parts of Eq. (26) are calculated from Eqs. (27) and (28).

$$F_{in} = \left[\frac{F_{in_0}^2}{F^n}\right]^{\left(\frac{1}{2-n}\right)}, \tag{27}$$

$$F_{st} = \left[\frac{F_{st_0}^2}{F^m}\right]^{\left(\frac{1}{2-m}\right)}. \tag{28}$$

The friction factors F_{in} and F_{st} are calculated by a method from Idel'cik.

$$\mathrm{Re} = \frac{M \cdot D_t}{\mu}, \tag{29}$$

$$F_{st_0} = 0.88 \cdot \left[\frac{2 \cdot a - 1}{\sqrt{a^2 + 0.25 \cdot b^2}} + 1\right]^2 \cdot \left[\frac{2 \cdot (a-1)}{2 \cdot a - 1}\right]^{1.73} \cdot \mathrm{Re}^m, \tag{30}$$

$$a = \frac{P_r}{D_t}, \tag{31}$$

$$b = \frac{P_l}{D_t}, \tag{32}$$

$$m = 0.295. \tag{33}$$

The exponent m is taken from the recommendations given in Ref. [33]. Furthermore:

$P_r \le P_l$:

$$F_{in_0} = 1.52 \cdot (a-1)^{-0.7} \cdot (b-1)^{0.2} \cdot \mathrm{Re}^n, \tag{34}$$

$$n = 0.2, \tag{35}$$

$P_r > P_l$:

$$F_{in_0} = 0.32 \cdot \left[\frac{a-1}{b-1} - 0.9\right]^{-0.68} \cdot (b-1)^{-0.5} \cdot \mathrm{Re}^n, \tag{36}$$

$$n = 0.2 \cdot \left[\frac{b-1}{a-1}\right]^2. \tag{37}$$

The expression for the friction factor given in Eq. (26) is implicit and has been solved in the model by using a second order Newton method with analytical derivatives.

Tube side heat transfer and pressure losses

On the tube side, high pressure single phase gas consisting of H_2 and refrigerant (also H_2 in this work) is cooled. In HX 2-HX 6, a low pressure H_2 single phase gas stream is heated in downward flow (as the shell side). The heat transfer coefficient is here calculated by using the Nu-correlation by Gnielinski [31]. Frictional pressure drops in tube j are predicted by the Blasius equation [37]:

$$\left(\frac{dp_j}{dz}\right)_f = f \cdot \frac{\dot{M}_j^2}{2 \cdot d \cdot \rho} \cdot \left(\frac{\mu_w}{\mu}\right)^{0.27} \tag{38}$$

Common model features

Some of the equations used are the same for the plate-fin and spiral-wound heat exchanger technologies. The steady-state mass balance of para-hydrogen for the streams flowing across catalyst is:

$$\frac{d\dot{m}_{H_2,p}}{dz} = A_{H_2}\, r_{o \to p}, \tag{39}$$

where $\dot{m}_{H_2,p}$ is the mass flow rate of para-hydrogen, A_{H_2} is the cross section area of a layer with catalyst pellets and $r_{o \to p}$ is the reaction rate per reactor volume per second for the forward reaction in Eq. (1). In previous work [7], we developed a

Please cite this article as: Skaugen G et al., Comparing exergy losses and evaluating the potential of catalyst-filled plate-fin and spiral-wound heat exchangers in a large-scale Claude hydrogen liquefaction process, International Journal of Hydrogen Energy, https://doi.org/10.1016/j.ijhydene.2019.12.076

correlation for the ortho-para conversion kinetics, $r_{o\rightarrow p}$ that reproduced available experimental data with an average deviation of 2.2%. In Ref. [7], we compared to all available experimental data on the conversion of ortho- and para-hydrogen. We refer to Ref. [7] for details about the expression for the reaction rate and for figures that display the comparison to the experimental data. The energy and momentum balances described previously were formulated in terms of the pressure and enthalpy. The advantage of this solution methodology is that the enthalpy of conversion between ortho and para-hydrogen is automatically taken into account. At each position, the temperature within a layer can be obtained by performing phase equilibrium calculations where the enthalpy and pressure are specified, as described in Ref. [38]. In this work, we used a nested loop approach to solve the enthalpy-pressure phase equilibrium calculations [39], employing the thermodynamic framework presented in Ref. [40]. The hydrogen was described as an ideal mixture between ortho and para-hydrogen at local equilibrium at each position z, where the EoS by Leachman et al. [10] was used to describe the thermodynamic properties of ortho and para-hydrogen. Thermal conductivities and viscosities of the nonequilibrium mixture of ortho- and para-hydrogen were computed with the corresponding state approach, TRAPP, with propane as the reference fluid.

We assume that in pipes or layers filled with catalyst, the heat transfer with the wall and the pressure drop is dominated by the characteristics of the pellets. Therefore, for the heat transfer coefficient, the correlations by Peters [41] was used. The pressure loss in the catalyst-filled tubes use the model by Ergun, by using the superficial gas flow in the bulk flow pressure loss but with a modified expression for the friction factor by Hicks [42]. The pellet void fraction is calculated from the model by Haughey and Beveridge [43].

The exergy destruction in the heat exchangers

We shall evaluate the exergy destruction due to irreversibilities that take place inside of the heat exchangers. For the heat exchangers discussed in this work, the exergy destruction and lost work originate from three contributions (See Ref. [7] for details):

$$\dot{E}_d=\dot{E}_T+\dot{E}_P+\dot{E}_{Rx}=\int_0^L\Bigg[\underbrace{\sum_{i=1}^{n}\sum_{k=1}^{n}T_0\gamma_{i,k,eff}J_{q,k,i}\left(\frac{1}{T_i}-\frac{1}{T_k}\right)}_{\dot{e}_T}\Bigg]dz$$
$$+\int_0^L\Bigg[\underbrace{\sum_{i=1}^{n}T_0A_iv_i\left(-\frac{1}{T_i}\frac{dp_i}{dz}\right)}_{\dot{e}_P}\Bigg]dz+\int_0^L\Bigg[\underbrace{\sum_{i=1}^{n}T_0A_ir_{o\rightarrow p}\left(-\frac{\Delta G_{o\rightarrow p,i}}{T_i}\right)}_{\dot{e}_{Rx}}\Bigg]dz, \quad (40)$$

where n is the total number of layers, T_0 is the reference temperature of the environment, taken in this work to be 298 K, $\gamma_{i,k}$ is the perimeter between stream k and i, $J_{q,i,k}$ denotes the heat flux from stream i to stream k, $\Delta G_{o\rightarrow p,i}$ is the Gibbs free energy of the ortho-para hydrogen conversion in stream i, $\dot{E}_T$, $\dot{E}_P$ and $\dot{E}_{Rx}$ represent the total exergy destruction within the heat exchanger from heat transfer, pressure drop and ortho-para hydrogen conversion respectively. Analogously, $\dot{e}_T$, $\dot{e}_P$ and $\dot{e}_{Rx}$ represent the local exergy destruction within the heat exchanger, with units of [W/m]. Further, $\gamma_{i,k,eff}=\gamma_{i,k}$ in the spiral-wound heat exchangers, and $\gamma_{i,k,eff}=0.5\gamma_{i,k}$ in the plate-fin heat exchangers. Note that for the layers where no ortho-para hydrogen conversion takes place, $r_{o\rightarrow p}=0$ and the last term on the right-hand-side of Eq. (40) is zero. The local entropy production that was used to compute the local exergy destruction in Eq. (40) can be derived similarly as in Ref. [44]. By analyzing the different terms in Eq. (40), one can identify the main sources and the location of the exergy destruction in the heat exchangers. Furthermore, the energy efficiency based on the second law of thermodynamics, η_{II} was computed by using the same approach as described in Ref. [45].

Result and discussion

In the following, we will compare the characteristics, behavior and performances of plate-fin and spiral-wound heat exchangers for use in a large-scale Claude refrigeration process for liquefaction of hydrogen.

While catalyst filled plate-fin heat exchangers is the present state-of-the-art, spiral-wound heat exchangers have not yet been considered for use in LH_2 production. Hence, this work presents an initial evaluation of their suitability for this purpose. The seven heat exchanger in the process are depicted in Fig. 1. Since the flooded evaporated (HX-7) has a low duty (0.2 MW) and operates in the two-phase regime, it will be omitted from the analysis. HX-7 should likely be designed as a compact plate heat exchanger.

The outlet pressures, ortho-para hydrogen conversion and temperatures differ slightly for plate-fin and spiral-wound heat exchangers. Therefore, we shall consider two processes; one where only plate-fin heat exchangers have been employed, and another where exclusively spiral-wound heat exchangers have been used. The exact boundary conditions for the heat exchangers in the two processes are reported in the Supplementary Information (SI). A key difference between the two processes is that only one shell-stream is possible in a spiral-wound heat exchanger, and the smallest cold stream flows in some of the pipes. This implies that while the outlet temperatures from the cold streams usually differ for the spiral-wound heat exchangers, they can be designed to be equal in a plate-fin heat exchanger.

The heat exchanger designs

The heat exchanger designs were determined by matching intermediate temperatures decided by the LH_2 process configuration (see the SI), while keeping the pressure drop of each stream of the heat exchangers below a defined value, typically 0.7 bar for the high pressure streams and 0.05 bar for medium and low pressure streams. Moreover, the designs were constrained by the maximum module dimensions that can be manufactured by commercial suppliers [8]. The dimensions of the plate-fin heat exchanger

Please cite this article as: Skaugen G et al., Comparing exergy losses and evaluating the potential of catalyst-filled plate-fin and spiral-wound heat exchangers in a large-scale Claude hydrogen liquefaction process, International Journal of Hydrogen Energy, https://doi.org/10.1016/j.ijhydene.2019.12.076

modules were kept within widths, heights and lengths of 1.5, 1.5 and 8 m respectively. The outer shell diameters of the spiral-wound heat exchangers were kept below 4.7 m. The designs have not been subject to optimization, but serve the purpose of facilitating a comparison of plate-fin and spiral-wound heat exchangers. Further optimization is beyond the scope of the present work, as this should be carried-out for the whole process. The resulting key geometrical parameters for the heat exchangers are displayed in Tables 2 and 3 for the plate-fin and spiral-wound heat exchangers respectively. All the plate-fin heat exchangers are 1.5 m wide, and the stacking sequences of the cold and hot streams are provided in the SI.

The surface density of a heat exchanger, η_s, denotes the available heat exchanger area per volume. The surface densities are summarized by the last columns in Tables 2 and 3, and vary between 100 and 300 m^{-1} for the spiral-wound heat exchangers and 950-1250 m^{-1} for the plate-fin heat exchangers, i.e. they are about 5–10 times higher for the plate-fin heat exchangers. The plate-fin heat exchangers are significantly more compact, which results in a smaller volumetric foot-print for a target duty. The weights of the spiral-wound heat exchangers are 2–14 times higher. The increase in weight is partly due to the lower surface density, but also because of a large increase in the necessary surface area between hot and cold streams, A_s. For all of the heat exchangers except HX-6, we find that a significantly larger surface area is needed in the spiral-wound heat exchanger to match the targeted intermediate temperatures of the LH_2 process.

In HX-3 to HX-6, some of the pipes and layers are filled with catalyst. This makes up about 30% of the total heat exchanger weight. This weight estimation did not account for the additional piping needed for the parallel plate-fin heat exchanger units. An advantage of using spiral-wound heat exchangers is the possibility to have only one unit for each heat exchanger. It is necessary to have between 1 (HX-6) and 4 parallel units (HX-2 and HX-5) if the plate-fin heat exchanger technology is chosen. This will lead to additional piping and extra weight.

The average helix angles of the first two spiral-wound heat exchangers are 12° and 16°. The average helix angle of the last four spiral-wound heat exchangers varies between 23° and 29°. The reason for the large increase in helix angle for the last heat exchangers is to restrict the total pressure drop, since pipes filled with catalyst have higher pressure drops than open pipes. The helix angle for the tube layers containing the catalyst is in the range 60–70°. The high helix angle makes it technically more feasible to fill catalytic pellets into the pipes. The helix angle for the high and low pressure gas streams are in the range 10–13° in order to provide the appropriate thermal length.

Distribution of heat exchanger duty and exergy destruction

The duty, exergy destruction and second law efficiencies, η_{II}, of the heat exchangers are presented in Table 4. The overall duty of both processes is almost the same. The slightly higher duty of the process with only spiral-wound heat exchangers (0.4 MW) is due to a higher conversion of ortho-hydrogen, where the outlet mole-fraction of para-hydrogen from HX-6 is 0.97 for the spiral-wound heat exchanger and 0.93 from the plate-fin heat exchanger. The conversion to para-hydrogen is very costly at the lowest temperatures.

We can exploit Eq. (40) from nonequilibrium thermodynamics [46] to categorize the exergy destruction as thermal, from fricional pressure drop or from conversion of ortho-to para-hydrogen. In the spiral-wound heat exchangers, the distribution between thermal, pressure-based and conversion-based exergy destruction is 84%, 14% and 2% respectively. The corresponding numbers for the plate-fin heat exchangers are 64%, 30% and 6%. The general trend is that the spiral-wound heat exchangers have a lower exergy destruction from pressure drop and ortho-para hydrogen conversion.

The overall distribution between the plate-fin heat exchangers is further illustrated in Fig. 4. The figure shows that even though about 81% of the heat exchanger duty is allocated to HX-1 and HX-2 in the precooling section, they are responsible for less than 45% of the total exergy destruction. The reason for this is that the exergy destruction increases proportionally with T^{-1}, which means that it is particularly parasitic at low temperatures. The last heat exchanger, HX-6 accounts for 2% of the overall duty, but is responsible for about 14% of the overall exergy destruction for the plate-fin heat exchanger designs.

The heat exchanger duties vary from about 1 MW in HX-6 to 31 MW in HX-2, while the exergy destruction increases from about 3 to 5% in HX-1 and HX-2 to 64% in HX-6. In the first two heat exchangers, the exergy destruction makes up a small percentage of the total duty. However, due to the large duties, a small relative improvement can lead to a significant reduction of the total exergy destruction. The last heat exchangers have much lower duties, but also a higher relative exergy destruction. Hence, it is relevant to address all of the six heat exchanger to improve the process.

The second law efficiencies of the heat exchangers vary between 72.3% and 96.6%. Although the exergy destruction

Table 2 – Key geometry parameters of the plate-fin heat exchangers.

Type	Length [m]	Height [m]	Nr parallel	Nr layers	Weight [ton]	$A_s \cdot 10^{-3}$ [m^2]	η_s [m^{-1}]
HX-1	3.51	2.19	2	330	14.63	14.6	1253.46
HX-2	5.01	4.94	4	660	45.43	47.3	1244.81
HX-3	0.41	1.85	2	210	3	1.1	948.5
HX-4	2.56	3.79	3	505	35.09	14.1	964.32
HX-5	3.01	5.48	4	800	46.01	28.2	1129.24
HX-6	1.26	1.37	1	160	7.63	2.8	1041.96

Please cite this article as: Skaugen G et al., Comparing exergy losses and evaluating the potential of catalyst-filled plate-fin and spiral-wound heat exchangers in a large-scale Claude hydrogen liquefaction process, International Journal of Hydrogen Energy, https://doi.org/10.1016/j.ijhydene.2019.12.076

Table 3 – Key geometry parameters of the spiral-wound heat exchangers.

Type	Height [m]	Diameter [m]	Helix angle	Nr layers	Nr tubes	Weight [ton]	$A_s \cdot 10^{-3}$ [m^2]	η_s [m^{-1}]
HX-1	15	4.66	12.37	120	26 363	172.32	69.4	271.39
HX-2	30	4.09	16.44	115	24 041	193.93	78.3	198.16
HX-3	2	3.36	28.95	72	9116	13.83	3.3	185.88
HX-4	18	4.49	28.03	120	21 871	259.8	54.9	192.29
HX-5	8	3.86	22.71	91	15 719	106.39	18.1	192.99
HX-6	3.25	3.17	29.32	71	9018	21.26	2.7	104.18

Table 4 – Exergy destruction in the plate-fin and spiral-wound heat exchangers.

The plate-fin heat exchangers

Type	Duty [MW]	$\dot{E}_T$ [kW]	$\dot{E}_P$ [kW]	$\dot{E}_{Rx}$ [kW]	$\dot{E}_d$ [kW]	Exergy dest. [%]	η_{II} [%]
HX-1	12.6	608.3	153.0	0	761.3	6.1	88.9
HX-2	31.3	1054.7	435.4	0	1490.1	4.8	91.9
HX-3	1.2	168.8	454.1	1.9	624.7	50.5	72.3
HX-4	5.0	619.7	357.3	28.0	1005.0	19.9	91.9
HX-5	2.7	241.8	66.1	79.4	387.3	14.2	96.6
HX-6	1.1	482.2	26.0	178.4	686.6	61.4	91.8
ALL	54.0	3176	1492	288	4955		

The spiral-wound heat exchangers

Type	Duty [MW]	$\dot{E}_T$ [kW]	$\dot{E}_P$ [kW]	$\dot{E}_{Rx}$ [kW]	$\dot{E}_d$ [kW]	Exergy dest. [%]	η_{II} [%]
HX-1	12.7	423.5	17.3	0	441	3.5	93.5
HX-2	31.4	835.9	178.8	0	1015	3.2	94.3
HX-3	1.5	172.1	135.4	1.9	309	20.1	88.3
HX-4	5.3	486.3	75.4	11.7	573	10.8	95.6
HX-5	2.7	412.1	53.2	27.4	493	18.2	96.0
HX-6	1.0	580.5	12.1	40.3	633	64.7	91.7
ALL	54.6	2910	472	81	3464		

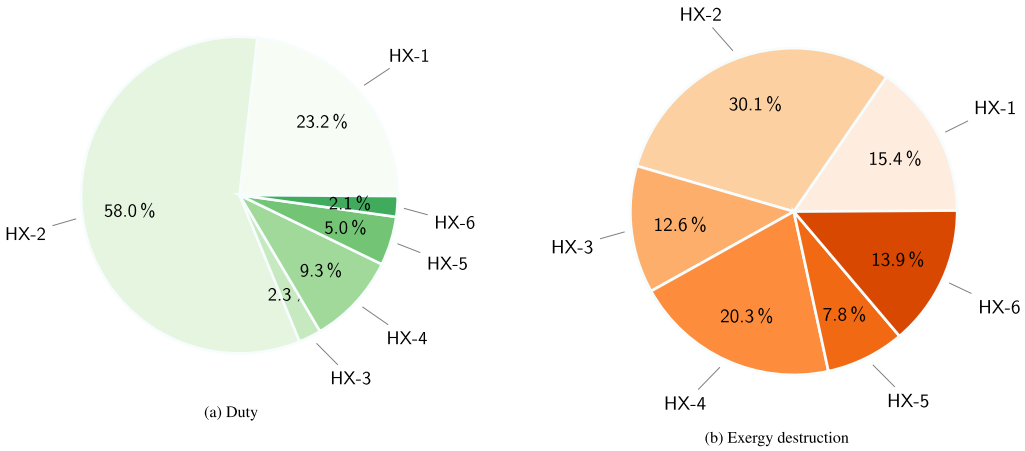

Fig. 4 – Distribution between of the duty (left) and the exergy destruction (right) for plate-fin heat exchangers, HX-1 to HX-6.

makes up a higher percent of the duty at lower temperatures, compare e.g. HX-1 and HX-6, the second law efficiencies do not follow this trend. This is because of the large entropic contribution to the change in exergy across the heat exchangers, which increases at lower temperatures.

In the following, we shall discuss each heat exchanger in more detail, and evaluate both the potential for improvement as well as the potential benefits of incorporating novel catalyst filled spiral-wound heat exchangers into the process.

HX-1

The purpose of HX-1 is to cool the H_2 feed stream and the high-pressure MR from ambient temperature to about 114 K by use of a low-pressure MR. The temperatures in the plate-fin heat exchanger are depicted in Fig. 5a. The corresponding temperature profiles for the spiral-wound heat exchanger look very similar and have not been shown. The figure displays a tight thermal match between the hot and cold

Please cite this article as: Skaugen G et al., Comparing exergy losses and evaluating the potential of catalyst-filled plate-fin and spiral-wound heat exchangers in a large-scale Claude hydrogen liquefaction process, International Journal of Hydrogen Energy, https://doi.org/10.1016/j.ijhydene.2019.12.076

streams, where the temperature differences vary between 1 K and 16 K.

Table 4 reveals that most of the exergy destruction in HX-1 originates in thermal gradients. Eq. (40) can be used to further identify the locations of the largest exergy destructions within the heat exchangers. Fig. 5 (bottom) illustrates the local exergy destruction in HX-1 as represented by the arguments of the integral in Eq. (40). The figure reveals that there are two main locations for thermal exergy destruction in both heat exchanger types; near at the hot-end ($z/L>0.9$), and near the middle. Near the hot end, the low-pressure MR leaves at a temperature that is 16 K below that of the H_2 feed and 13 K lower than the high pressure MR, creating a thermal mismatch and thermal exergy destruction. The vapor-fraction plotted in Fig. 5b shows that near the middle of the plate-fin heat exchanger, the condensing high-pressure MR exits the two-phase region and becomes single-phase liquid. When the high-pressure MR condenses, latent heat is released, which helps to maintain the temperature of the stream. After the two-phase high-pressure MR becomes single-phase liquid, the temperature starts to drop more rapidly, as can be seen by the temperature slope in Fig. 5a. This creates a thermal mismatch, which is the origin of the hump near the middle of Fig. 5c, d.

A possible strategy to reduce this exergy destruction is to employ a dual or cascade MR process, which is state of the art in LNG production [47]. A key argument for this is that HX-1 has a temperature span of more than 150 K, which is comparable to the temperature span encountered in LNG production. A more sophisticated process with multiple MR compositions has the potential to significantly reduce the exergy destruction in HX-1, since the use of more MR compositions enables the refrigerant to be in the two-phase regime throughout the entire heat exchanger, as well as a better match of the inlet temperatures of high-pressure MR and the H_2 feed.

A challenge that must be addressed before employing single or multiple MR processes for hydrogen liquefaction is the possible occurrence of flow-instabilities such as Ledinegg instabilities. They can cause large thermal oscillations and obstruct the heat exchanger [27]. Further discussion of such challenges is beyond the scope of the present work.

HX-2

HX-2 is the largest heat exchanger in the process, with a duty of 31 MW. As a consequence, it is responsible for about one third of the total exergy destruction. The purpose of HX-2 is to cool the high pressure H_2 refrigerant from ambient temperature to 119 K, as shown in Fig. 6a. Here, both the low- and medium-pressure H_2 refrigerants are cold streams. The performances of the plate-fin and the spiral-wound heat exchangers are similar, where both temperature gradients and pressure drop are important sources of exergy destruction. The smaller exergy destruction and higher second law efficiency in the spiral-wound heat exchanger is due to the significantly larger volume and surface area, A_s.

We shall next discuss the exergy destruction in HX-2 and possible ways to reduce it. Since the spiral-wound heat exchanger behaves qualitatively similar to the plate-fin heat exchanger, we display only results from the plate-fin heat

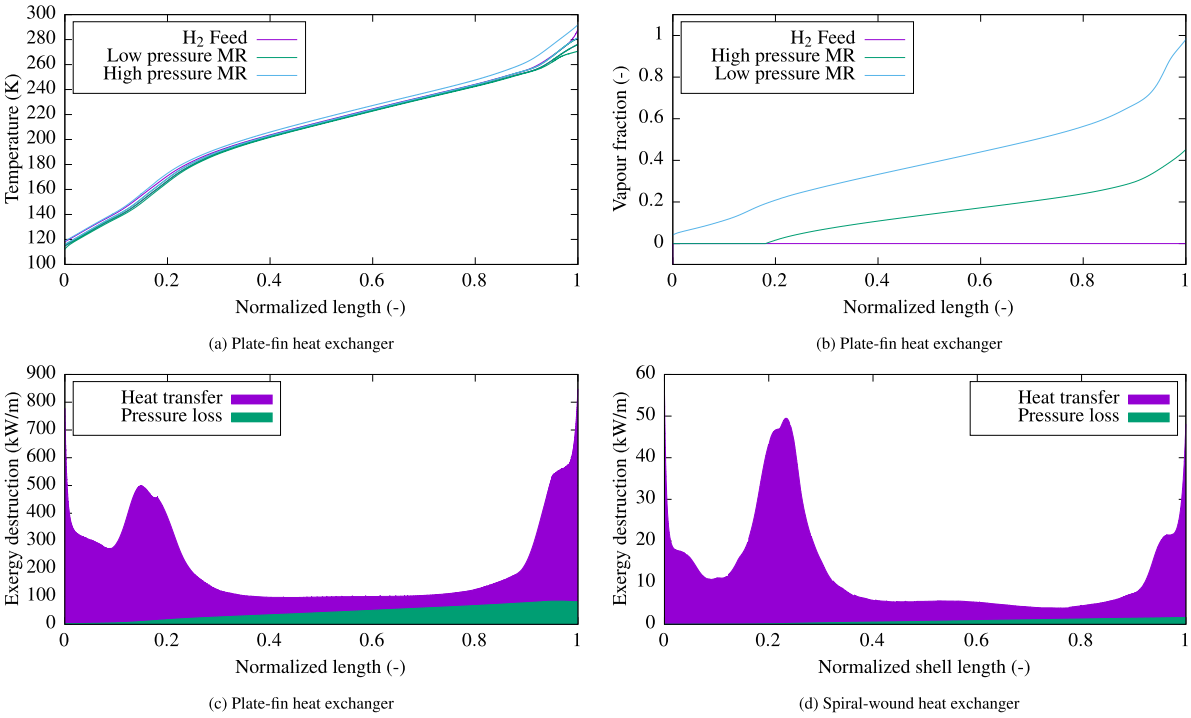

Fig. 5 – The temperatures and vapor-fractions for the streams of HX-1 are shown for the plate-fin heat exchanger in the top figures. The corresponding results from the spiral-wound heat exchanger are very similar and have not been shown. The solid lines are the stream temperatures and the dashed lines represent the wall temperatures. The bottom figures display the local exergy destruction in the plate-fin and spiral-wound heat exchangers.

Please cite this article as: Skaugen G et al., Comparing exergy losses and evaluating the potential of catalyst-filled plate-fin and spiral-wound heat exchangers in a large-scale Claude hydrogen liquefaction process, International Journal of Hydrogen Energy, https://doi.org/10.1016/j.ijhydene.2019.12.076

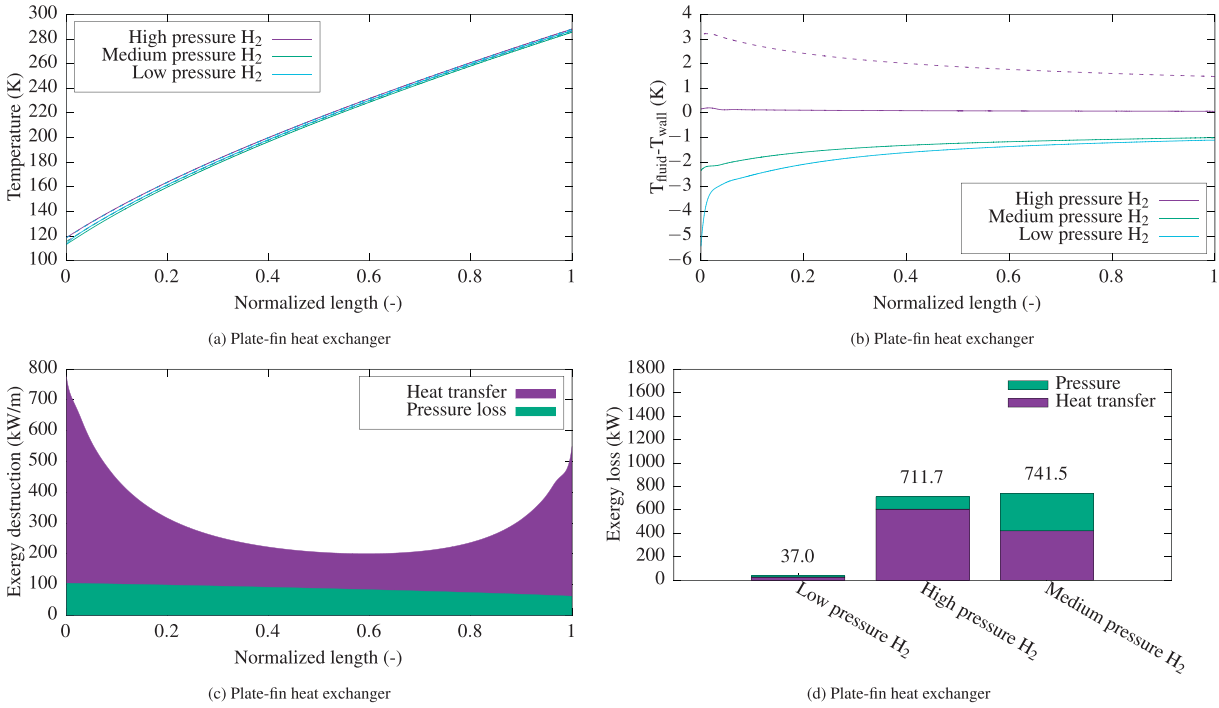

Fig. 6 – The temperature profiles through HX-2 for the plate-fin heat exchanger are shown in the top figure. Here, the solid lines are the stream temperatures and the dashed lines represent the wall temperatures in Fig. 6a and the temperature difference between the H2HP fluid and H2MP wall in Fig. 6b. The bottom figures show the local exergy destruction.

exchanger. Fig. 6d shows that most of the exergy destruction in HX-2 comes from the medium and high-pressure H_2 streams. The total mass-flow rate of the low-pressure H_2 is more than 20 times smaller than the other streams and is only present in 1/6 of the total number of layers. Even with a low fin density and perforated fins, the temperature follows closely the profile of the warm high pressure H_2 stream. The near-zero temperature difference is shown by the solid magenta line in Fig. 6b. The exergy destruction both from thermal gradients and pressure gradients is higher in the medium pressure H_2 due to a lower density than in the high pressure H_2. We find that the wall heat transfer coefficient of the medium pressure hydrogen is on average 45% lower than that of the high pressure hydrogen. This explains the larger temperature difference in Fig. 6b and the larger exergy destruction from this stream.

In Ref. [48], we showed that a good strategy to lower the entropy production/exergy destruction in a heat exchanger in the hydrogen liquefaction process is to modify the design and operation such that the local exergy destruction is equally distributed in space. An inspection of the local exergy destruction of HX-2 displayed in Fig. 6c shows that this is far from the case. The exergy destruction in the heat exchanger is much larger near the cold end than near the warm end. This can be explained from the temperature differences, which are also largest near the cold-end, as shown in Fig. 6a, b. The situation can be improved by modifying the heat exchanger design to facilitate equipartition of the local exergy destruction. In the spiral-wound heat exchanger, the helix angle of the wounded pipes could be modified near the cold end in order to have a higher surface density. In the plate-fin heat exchanger, different fin specifications could be used near the cold and hot ends. However, further optimization of these configurations is beyond the scope of the present work.

HX-3, HX-4 and HX-5

In HX-3 to HX-6, the layers and pipes where H_2 feed flows are filled with catalyst. The catalyst gives a higher pressure drop, but enhances the heat transfer, as discussed in detail in Ref. [7]. In HX-4 and HX-5 most of the exergy destruction comes from the medium pressure H_2 while in HX-3, most of the exergy destruction comes from the high pressure H_2. The exergy destruction from the ortho-para conversion is found to be relatively small (see Table 4), in particular in the spiral-wound heat exchangers. For HX-3 and HX-4, the total exergy destruction in the plate-fin heat exchangers is significantly larger than in the spiral-wound heat exchangers. The main reason for this is the much larger exergy destruction from the pressure drop, which constitutes about 72% of the total exergy destruction in plate-fin heat exchanger HX-3. The pressure drop in this plate-fin heat exchanger is 0.7 bar for the high pressure H_2 and 0.06 bar for the medium pressure H_2. Despite the much lower pressure drop, 30% of the exergy destruction comes from the medium pressure refrigerant, as shown in Fig. 7a. In comparison, the pressure drop in the spiral-wound heat exchanger is 0.1 bar for the high-pressure H_2 and 0.00 bar for the medium pressure H_2, i.e. much lower. The situation can be improved by increasing the number of layers with high and medium pressure refrigerant in the plate-fin heat

Please cite this article as: Skaugen G et al., Comparing exergy losses and evaluating the potential of catalyst-filled plate-fin and spiral-wound heat exchangers in a large-scale Claude hydrogen liquefaction process, International Journal of Hydrogen Energy, https://doi.org/10.1016/j.ijhydene.2019.12.076

exchanger or by increasing the fin-height. The framework presented in this paper, in particular Eq. (40), allows the exergy destruction to be located and identified. Furthermore, it makes it possible to compare different sources of exergy destruction on equal terms and enables a qualified specification on the maximum allowed pressure drops in the streams, as they are directly linked to the exergy destruction. In this respect, the maximum allowed pressure drop should probably be decreased in HX-3 to increase the efficiency of the plate-fin heat exchanger, which has the lowest second law efficiency of all the heat exchangers (72.3%).

HX-6

HX-6 has the lowest duty of the heat exchangers considered (2% of the overall duty), but accounts for a significant part of the total exergy destruction, as shown in Fig. 8b. The purpose of HX-6 is to cool the H_2 feed from 43 K to 29.7 K, where the temperature profiles are illustrated in Fig. 8 (top).

The are two locations in HX-6 with pronounced thermal mismatches between the hot and cold streams; near the cold end, and at a location near $z/L = 0.3$ in the plate-fin heat exchanger and near $z/L = 0.5$ in the spiral-wound heat exchanger. Fig. 8e, f show that the mismatch accounts for a large part of the total exergy destruction.

The low-pressure H_2 enters HX-6 at about 22 K as single-phase gas. However, due to a higher pressure (about 8 bar), the saturation temperature of the other cold stream, the medium-pressure H_2 is 30 K. The difference between the temperatures of these streams creates a thermal mismatch near the cold end. The second thermal mismatch stems from a peak in the heat capacity of the H_2 feed near the critical region. Possible routes to reduce the thermal exergy destruction of HX-6 are to use a different refrigerant such as novel helium-neon-hydrogen mixtures, or increase the pressure of the H_2 feed gas.

A comparison of Fig. 8e with 8f reveals that the exergy destruction from the ortho-para hydrogen conversion (blue shaded area) is much smaller in the spiral-wound heat exchanger than in the plate-fin heat exchanger. This can be understood by investigating Fig. 8c, d, which compare the mole-fraction of para-hydrogen in the stream and the equilibrium value at the H_2 feed temperature. The H_2 feed stream in the spiral-wound heat exchanger has a composition that is much closer to the equilibrium composition at the stream temperature. This results in both lower exergy destruction as well as a higher outlet mole fraction of para-hydrogen. The reason for the improved conversion is the lower compactness of the spiral-wound heat exchanger. The lower surface density results in a higher residence time for a given duty, and a more favorable reaction rate to heat transfer rate ratio. The increased residence time is particularly beneficial for the ortho-para conversion as the reaction is rather slow, even in the presence of catalyst.

An overall view of the conversion through all the heat exchangers in the process is displayed in Fig. 9. The figure reveals that the spiral-wound heat exchangers bring the feed H_2 significantly closer to its equilibrium para-hydrogen composition throughout the entire process.

Table 3 shows that the average helix angle in the spiral-wound HX-3 to HX-6 is larger (above 20° for the average and above 55° for the feed stream layer) than in HX-1 to HX-2, in order to keep the pressure drop of the H_2 feed stream within acceptable limits. However, Fig. 8f reveals that very little of the exergy destruction in HX-6 comes from the pressure drop. Hence, there is a possibility to decrease the helix-angle for the feed layer and accept a higher pressure loss to achieve a higher surface density and shorter heat exchangers.

General comments on the heat exchanger designs

Preliminary heat exchanger designs have been presented for the six main heat exchangers of a large-scale hydrogen liquefaction process, with the aim of reaching target intermediate temperatures for the streams in the process while keeping the geometric designs within boundaries set by the manufacturers and pressure drops within predefined limits. The results however, reveal a large potential for improvement that can be realized in future optimization studies. For instance, in HX-1 there are large thermal mismatches that should be addressed in future process design, e.g. by employing a dual or cascade mixed refrigerant process.

A comparison of the exergy destruction in the two types of heat exchangers shows that, except in HX-5 and HX-6, the spiral-wound heat exchangers outperform the plate-fin heat exchangers. However, this is misleading, as the weight and

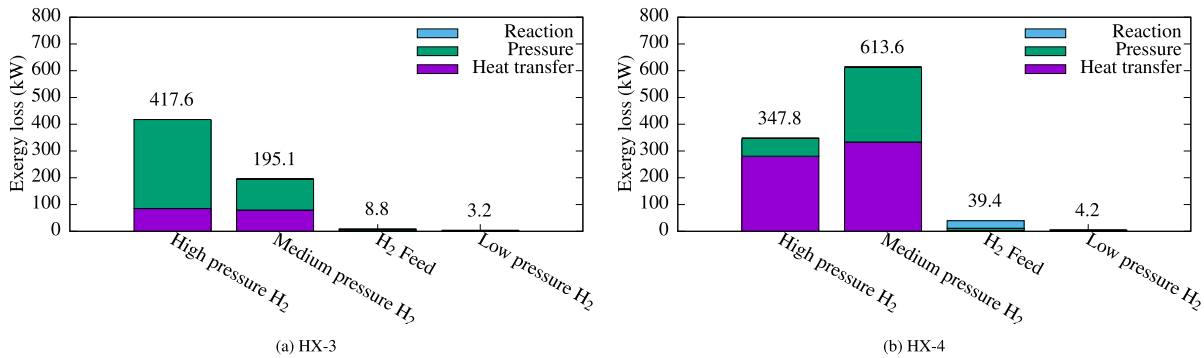

Fig. 7 – The distribution between the different contributions to the streams to the exergy destruction in the plate-fin heat exchangers, HX-3 and HX4.

Please cite this article as: Skaugen G et al., Comparing exergy losses and evaluating the potential of catalyst-filled plate-fin and spiral-wound heat exchangers in a large-scale Claude hydrogen liquefaction process, International Journal of Hydrogen Energy, https://doi.org/10.1016/j.ijhydene.2019.12.076

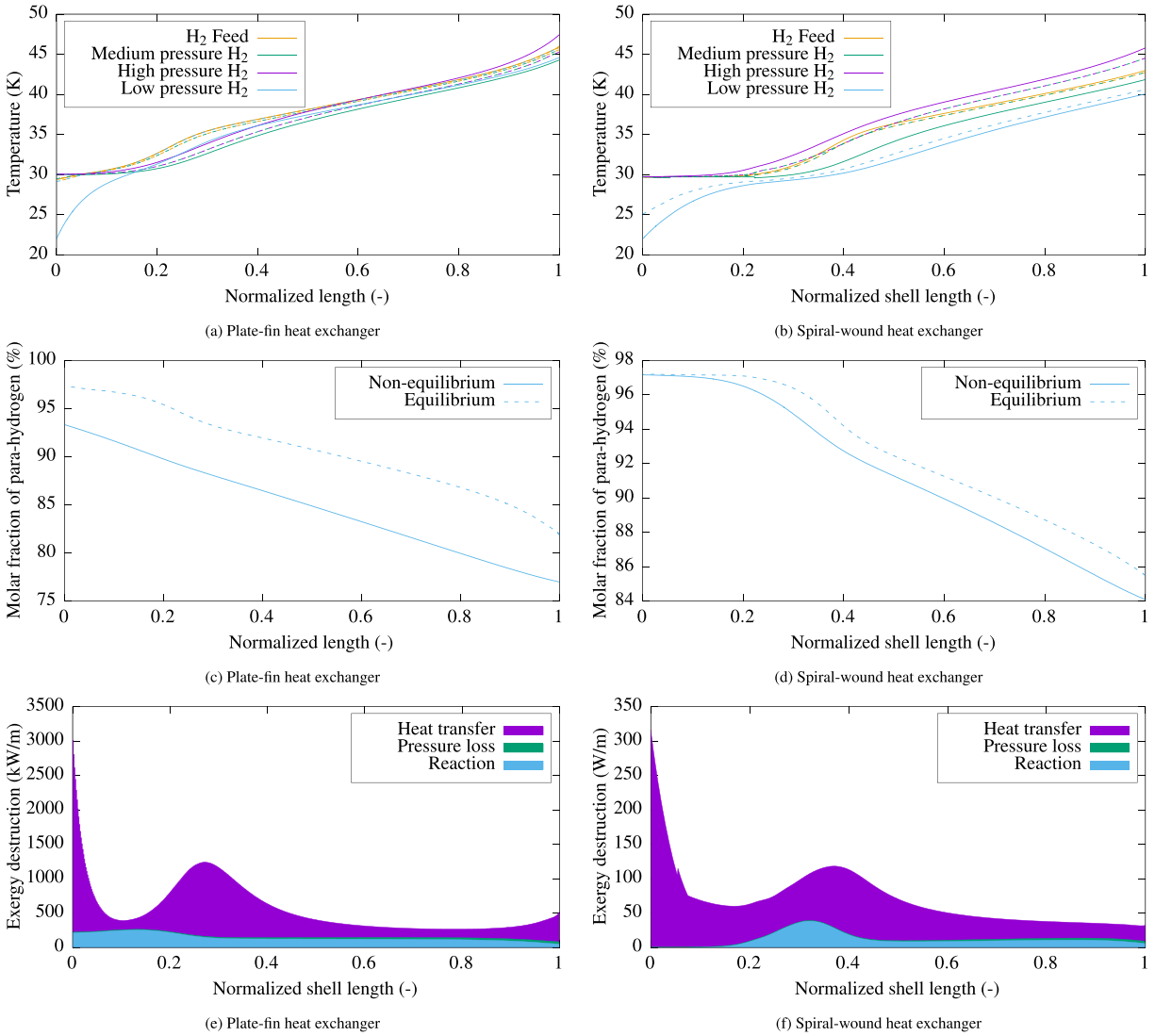

Fig. 8 – The temperatures (top), the mole fraction of para hydrogen (mid) and the local exergy destruction in HX-6. Here, the solid lines are either the stream temperatures (top) or the mole fraction of para hydrogen (mid). The dashed lines are either the wall temperatures (top) or the equilibrium mole fraction at the feed stream temperature (mid).

the surface areas, A_s, are several times larger for the spiral-wound heat exchangers (compare Tables 2 and 3). It is always possible to increase the number of parallel plate-fin heat exchanger configurations and thus the surface area to achieve lower exergy destruction. However, it is not possible to reduce the size of the spiral-wound heat exchanger much beyond the sizes in Table 3 and still match the intermediate temperatures in the process.

To gain further insight on the influence of heat exchanger size on the results, we investigated spiral-wound heat exchangers with the same boundary conditions as in HX-1 and HX-2. If the length of HX-1 was reduced by 50%, the outlet temperatures of the H_2 feed and the high pressure MR changed by only 2.5 K and 1.5 K respectively. A 50% reduction of the length of HX-2 increased the outlet temperature of the high pressure H_2 by 2.5 K. In both cases, the exergy destruction increased by about 50%, i.e. to an exergy destruction similar that of the plate-fin heat exchangers. We find that the last degrees of cooling of the streams are particularly costly, in particular for the spiral-wound heat exchangers. The large increase in the required heat exchanger area in the spiral-wound heat exchangers is both due to the lower surface density and lower heat transfer coefficients.

The state-of-the-art technology, plate-fin heat exchangers, is likely the best choice for the heat exchangers of a large-scale Claude refrigeration LH_2 process. In the cryogenic part, helium-neon-hydrogen mixtures have been proposed as novel mixed refrigerants that can enable the use of highly efficient turbo compressor equipment, as well as evaporate at the cold-side of the heat exchangers [8,9]. Evaporation will enhance the heat transfer, which will shift the para-hydrogen composition of the stream even further away from equilibrium. Unless a significantly improved catalyst is developed, the spiral-wound heat exchanger technology could be

Please cite this article as: Skaugen G et al., Comparing exergy losses and evaluating the potential of catalyst-filled plate-fin and spiral-wound heat exchangers in a large-scale Claude hydrogen liquefaction process, International Journal of Hydrogen Energy, https://doi.org/10.1016/j.ijhydene.2019.12.076

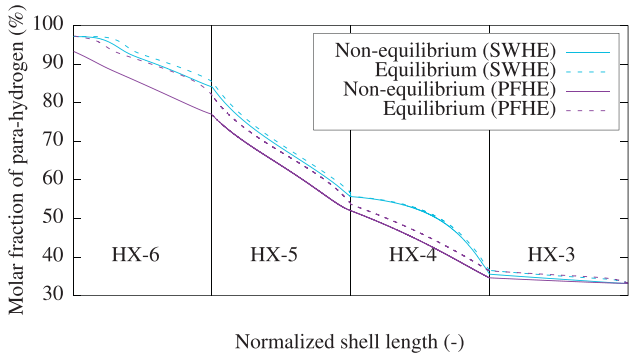

Fig. 9 – The mole fraction of para-hydrogen trough the process (solid lines) compared to the equilibrium para-hydrogen composition (dashed lines). The spiral-wound heat exchanger is represented by blue lines, and the plate-fin heat exchanger is represented by pink lines. The mole fraction of para H_2 is closer to the equilibrium composition at the H_2 feed temperature through the entire process. In the above figure, SWHE refers to the spiral-wound heat exchanger and PFHE refers to the plate-fin heat exchanger.

advantageous in the bottom part of such a process as it gives a longer residence time which allows for sufficient conversion of ortho-to-para hydrogen.

Conclusion

The state-of-the-art technology used in present hydrogen liquefaction processes is catalyst-filled plate-fin heat exchangers. An alternative that is commonly employed in large-scale processes for liquefaction of natural gas is spiral-wound heat exchangers, where several layers of (mostly hot) streams flow in pipes wounded around an inner mandrel, and the refrigerant flows counter-currently at the shell side.

In this work, we have presented mathematical models for catalyst filled plate-fin and spiral-wound heat exchangers and compared, for the first time, the performance of these two technologies for a large-scale Claude refrigeration process for liquefaction of hydrogen with a capacity of 125 tons/day. Design specifications for the six main heat exchangers were presented, both for the plate-fin and the spiral-wound heat exchanger technologies and detailed maps of the local exergy destruction were discussed for some of the heat exchangers. The heat exchanger duties varied between 1 and 31 MW and the exergy destruction made up between 3% and 64% of the duties. Their second law efficiencies varied between 72.3% and 96.6%. The exergy destruction in the heat exchangers decreased at lower temperatures, but their second law efficiencies did not follow this trend.

Because of geometrical constraints imposed by the heat exchanger manufacturers, we found that between 1 and 4 parallel plate-fin heat exchanger modules were required to achieve the desired capacity. Only one module was needed for each spiral-wound heat exchanger. Due to a lower surface density and heat transfer coefficients in the spiral-wound heat exchangers, their weights were 2–14 times higher than those of the plate-fin heat exchangers. While it was possible to employ more parallel plate-fin heat exchangers to increase the surface area and thus lower the exergy destruction, it was not possible to reduce the size of the spiral-wound heat exchangers much beyond what was reported and still match the intermediate temperatures of the process. In the spiral-wound heat exchangers, the distribution between thermal, pressure-based and ortho-para hydrogen conversion-based exergy destruction was 84%, 14% and 2% respectively. The corresponding numbers for the plate-fin heat exchangers were 64%, 30% and 6%. The general trend was that the spiral-wound heat exchangers had a lower exergy destruction from pressure drop and ortho-para hydrogen conversion.

In the first heat exchanger, H_2 feed gas was cooled from ambient temperature to about 120 K by use of a mixed refrigerant. Here, most of the exergy destruction occurred when the high-pressure mixed refrigerant entered the single-phase regime. A dual mixed refrigerant or a cascade process holds the potential to remove a large part of this exergy destruction and improve the efficiency. In many of the heat exchangers, we found an uneven local exergy destruction, which reveals a potential for further optimization of geometrical parameters. The framework presented allows a reasonable specification of the maximum allowed pressure drop through the heat exchangers, as the pressure drop is linked directly to the exergy destruction.

The mole-fraction of para-hydrogen was significantly closer to the equilibrium composition through the entire process for the spiral-wound heat exchangers. This was due to the longer residence time. As a consequence, the outlet mole fraction of para-hydrogen from the last spiral-wound heat exchanger was higher (0.97) than that from the last plate-fin heat exchanger (0.93). The exergy destruction from the conversion from ortho-to para-hydrogen was also lower.

Due to the higher surface densities of the plate-fin heat exchangers, they are the preferred technology for hydrogen liquefaction, unless a higher conversion to heat exchanger ratio is desired. Such a situation could occur in the bottom part of LH_2 processes if a boiling refrigerant of hydrogen-neon-helium mixtures is employed.

Acknowledgment

This publication is based on results from the research project Hyper, performed under the ENERGIX programme. The authors acknowledge the following parties for financial support: Equinor, Shell, Kawasaki Heavy Industries, Linde Kryotechnik, Mitsubishi Corporation, Nel Hydrogen, Gassco and the Research Council of Norway (255107/E20).

REFERENCES

[1] Evers AA. The hydrogen society - more than just a vision? Germany: Hydrogeit Verlag; 2017.

[2] Voldsund M, Jordal K, Anantharaman R. Hydrogen production with CO2 capture. Int J Hydrogen Energy 2016;41(9):4969–92.
[3] Burheim OS. Engineering energy storage. London, United Kingdom: Elsevier; 2017.
[4] Berstad DO, Stang JH, Nekså P. Large-scale hydrogen liquefier utilising mixed-refrigerant pre-cooling. Int J Hydrogen Energy 2010;35(10):4512–23.
[5] Yanxing Z, Maoqiong G, Yuan Z, Xueqiang D, Jun S. Thermodynamics analysis of hydrogen storage based on compressed gaseous hydrogen, liquid hydrogen and cryo-compressed hydrogen. Int J Hydrogen Energy 2019;44:16833–40.
[6] Kawasaki Heavy. Industries, Hydrogen value chains – scale and potential. Norway: gassconference; 2018.
[7] Wilhelmsen Ø, Berstad D, Aasen A, Nekså P, Skaugen G. Reducing the exergy destruction in the cryogenic heat exchangers of hydrogen liquefaction processes. Int J Hydrogen Energy 2018;43(10):5033–47.
[8] Report on technology overview and barriers to energy- and cost-efficient large scale hydrogen liquefaction. FCH JU FP7-JTI Project, Tech. Rep. Ref. 278177 D1.1. IDEALHY Consortium; 2012.
[9] Cardella U, Decker L, Klein H. Economically viable large-scale hydrogen liquefaction. IOP conference series: materials science and engineering, vol. 171; 2017, 012012.
[10] Leachman JW, Jacobsen RT, Penoncello SG, Lemmon EW. Fundamental equations of state for parahydrogen, normal hydrogen, and orthohydrogen. J Phys Chem Ref Data 2009;38:721.
[11] Ding C, Hu H, Ding G, Chen J, Mi X, Yu S. Influences of tube pitches on heat transfer and pressure drop characteristics of two-phase propane flow boiling in shell side of lng spiral wound heat exchanger. Appl Therm Eng 2018;131:270–83.
[12] Gilli PV. Heat transfer and pressure drop for cross flow through banks of multistart helical tubes with uniform inclinations and uniform longitudinal pitches. Nucl Sci Eng 1965;22(3):298–314.
[13] Lu X, Du X, Zeng M, Wang Q. Shell-side thermal-hydraulic performances of multilayer spiral-wound heat exchangers under different wall thermal boundary conditions. Appl Therm Eng 2014;70:1216–27.
[14] Ding C, Hu H, Ding G, Chen J, Mi X, Yu S, Li J. Experimental investigation on downward flow boiling heat transfer characteristics of propane in shell side of lng spiral wound heat exchanger. Int J Refrig 2017;84:13–25.
[15] Skaugen G, Kolsaker K, Walnum HT, Wilhelmsen Ø. A flexible and robust modelling framework for multi-stream heat exchangers. Comput Chem Eng 2013;49:95–104.
[16] Sanaye S, Hajabdollahi H. Thermal-economic multi-objective optimization of plate fin heat exchanger using genetic algorithm. Appl Energy 2010;87:1893–902.
[17] Phu NM, Trinh NTM. Modelling and experimental validation for off-design performance of the helical heat exchanger with lmtd correction taken into account. J Mech Sci Technol 2016;30:3357–64.
[18] Johannessen E. The state of minimum entropy production in an optimally controlled system. Ph.D. thesis. Norwegian University of Science and Technology; 2004.
[19] Hesselgreaves JE. Compact heat exchangers. Oxford: Pergamon Press; 2001.
[20] Khoshvaght-Aliabadi M, Zangouei S, Hormozi F. Performance of a plate-fin heat exchanger with vortex-generator channels: 3d-cfd simulation and experimental validation. Int J Therm Sci 2015;88:180–92.
[21] Lu X, Zhang G, Chen Y, Wang Q, Zeng M. Effect of geometrical parameters on flow and heat transfer performances in multi-stream spiral-wound heat exchangers. Appl Therm Eng 2015;89:1104–16.
[22] Wen J, Li Y, Zhou A, Zhang K. An experimental and numerical investigation of flow patterns in the entrance of plate-fin heat exchanger. Int J Heat Mass Transf 2006;49:1667–78.
[23] Valenti G, Macchi E. Proposal of an innovative, high-efficiency, large-scale hydrogen liquefier. Int J Hydrogen Energy 2008;33:3116–21.
[24] Ahmadi P, Hajabdollahi H, Dincer I. Cost and entropy generation minimization of a cross-flow plate fin heat exchanger using multi-objective genetic algorithm. J Heat Transf 2010;133:021801.
[25] Yousefi M, Enayatifar R, Darus AN. Optimal design of plate-fin heat exchangers by a hybrid evolutionary algorithm. Int Commun Heat Mass Transf 2012;39:258–63.
[26] Donaubauer PJ, Cardella U, Decker L, Klein H. Kinetics and heat exchanger design for catalytic ortho–para hydrogen conversion during liquefaction. Chem Eng Technol 2019;42:669–79.
[27] Skaugen G, Hammer M, Wahl P, Wilhelmsen Ø. Constrained non-linear optimisation of a process for liquefaction of natural gas including a geometrical and thermo-hydraulic model of a compact heat exchanger. Comput Chem Eng 2015;73.
[28] Bischoff S, Decker L. First operating results of a dynamic gas bearing turbine in an industrial hydrogen liquefier. AIP Conference Proceedings 2010;1218:887.
[29] Manglik R, Bergels A. Heat transfer and pressure drop correlations for the rectangular offset strip fin compact heat exchanger. Exp Therm Fluid Sci 1995;10(2):171–80.
[30] Bird RB, Stewart WE, Lightfoot EN. Transport phenomena. New York: John Wiley & Sons; 2007.
[31] Gnielinski V. New equations for heat and mass transfer in the turbulent flow in pipes and channels. Forsch Im Ingenieurwes 1975;41:8–16.
[32] Filonenko FK. Hydraulic resistance in pipes (in Russian). Teploenergetika 1954;1:40–4.
[33] Aunan B. Shell-side heat transfer and pressure drop in coil-wound lng heat exchangers,laboratory measurements and modeling. Ph.D. thesis. The Norwegian University of Science and Technology; 2000.
[34] Tang Q, Chen G, Yang Z, Shen J, Gong M. Numerical investigation on gas flow heat transfer and pressure drop in the shell side of spiral-wound heat exchangers. Sci China Technol Sci 2018;61(4):506–15.
[35] Smith EM. Design of helical-tube multistart coil heat exchangers. Advances in heat exchanger design of ASME winter meeting, vol. 6; 1986. 85, 1986.
[36] Barbe CD, Mordillat RD. Pertes de charge en écoulement monophasique et diphasique dans la calandre des échangeurs bobinés. In: 12ée Journées de l'Hydraulique; 1972.
[37] Blasius PRH. Das aehnlichkeitsgesetz bei reibungsvorgangen in flüssigkeiten. Forschung 1913;131:1–41.
[38] Michelsen ML, Mollerup JM. Thermodynamic models: {F} undamentals and computational aspects. 2nd ed. Holte, Denmark: Tie-Line Publictions; 2007.
[39] Wilhelmsen Ø, Skaugen G, Hammer M, Wahl PE, Morud JC. Time efficient solution of phase equilibria in dynamic and distributed systems with differential algebraic equation solvers. Ind Eng Chem Res 2013;52:2130–40.
[40] Wilhelmsen Ø, Aasen A, Skaugen G, Aursand P, Austegard A, Aursand E, Gjennestad M, Lund H, Linga G, Hammer M. Thermodynamic Modeling with Equations of State: present challenges with established methods. Ind Eng Chem Res 2017;56(13):3503–15.
[41] Peters PE, Schiffino RS, Harriott P. Heat transfer in packed-tube reactors. Ind Eng Chem Res 1988;27:226–33.

Please cite this article as: Skaugen G et al., Comparing exergy losses and evaluating the potential of catalyst-filled plate-fin and spiral-wound heat exchangers in a large-scale Claude hydrogen liquefaction process, International Journal of Hydrogen Energy, https://doi.org/10.1016/j.ijhydene.2019.12.076

[42] Hicks RE. Pressure drop in packed beds of spheres. Ind Eng Chem Fundam 1970;9(3):500–2.
[43] Haughey DP, Beveridge GSG. Structural properties of packed beds – a review. Can J Chem Eng 1969;42:130–40.
[44] Wilhelmsen Ø, Johannessen E, Kjelstrup S. Energy efficient reactor design simplified by second law analysis. Int J Hydrogen Energy 2010;35(24):13219–31.
[45] Mehdizadeh-Fard M, Pourfayaz F. Advanced exergy analysis of heat exchanger network in a complex natural gas refinery. J Clean Prod 2019;206:670–87.
[46] Kjelstrup S, Bedeaux D. Non-equilibrium thermodynamics of heterogeneous systems. Singapore: World Scientific; 2008.
[47] Khan MS, Karimi IA, Lee M. Evolution and optimization of the dual mixed refrigerant process of natural gas liquefaction. Appl Therm Eng 2016;96:320–9.
[48] Hånde RA, Wilhelmsen Ø. Minimum entropy generation in a heat exchanger in the cryogenic part of the hydrogen liquefaction process: on the validity of equipartition and disappearance of the highway. Int J Hydrogen Energy 2019;44:15045–55.

Please cite this article as: Skaugen G et al., Comparing exergy losses and evaluating the potential of catalyst-filled plate-fin and spiral-wound heat exchangers in a large-scale Claude hydrogen liquefaction process, International Journal of Hydrogen Energy, https://doi.org/10.1016/j.ijhydene.2019.12.076